Terr. Atmos. Ocean. Sci., Vol. 29, No. 1, 39-50, February 2018 doi: 10.3319/TAO.2017.07.04.01

Imaging P- and S-wave velocity structures in hydrate bearing sediments along an OBS profile across the Yuan-An Ridge, off southwest Taiwan

Win-Bin Cheng[1,*], Yi-Ru Wu[1], Chin-Wei Liang[2], Jing-Yi Lin[2], and Shu-Kun Hsu[2]

[1] *Department of Environment and Property Management, Jinwen University of Science and Technology, New Taipei City, Taiwan*
[2] *Department of Earth Sciences, National Central University, Taoyuan City, Taiwan*

Article history:
Received 1 October 2016
Revised 2 July 2017
Accepted 4 July 2017

Keywords:
Marine slope instability, Ocean bottom seismometer, Seismic velocity

Citation:
Cheng, W.-B., Y.-R. Wu, C.-W. Liang, J.-Y. Lin, and S.-K. Hsu, 2018: Imaging P- and S-wave velocity structures in hydrate bearing sediments along an OBS profile across the Yuan-An Ridge, off southwest Taiwan. Terr. Atmos. Ocean. Sci., 29, 39-50, doi: 10.3319/TAO.2017.07.04.01

ABSTRACT

In order to improve our understanding of the marine slope instability of hydrate-bearing sediments in the offshore southwestern Taiwan, P- and S-waves seismic data generated by P-S conversion on reflection from airgun shots recorded from a multi-component Ocean Bottom Seismometer (OBS) survey were used to construct two-dimensional velocity model. The investigated profile lies above a structural high of the Yuan-An ridge, proposed as a high priority drilling site for gas hydrate investigations off southwest Taiwan. The locations of the OBSs were determined with high accuracy by an inversion based on the shot traveltimes. Traveltime inversion and forward modeling of seismic data result in general trends P- and S-wave velocities of sediments. Generally, P- and S-wave velocities are high beneath topographic ridges which might represent a series of thrust-cored anticlines develop in the accretionary wedge. P-wave velocities of the sea floor are about ~1.58 km s^{-1}, increasing to the bottom simulating reflectors (BSR), reaching values of about ~2 km s^{-1}. Below it, a low velocity layer (1.62 - 1.74 km s^{-1}) is observed, which indicates the presence free gas in the sedimentary layer. S-wave velocities of the sediments over the entire section range from 0.3 to ~0.6 km s^{-1}. Significant lateral velocity variations were found beneath the eastern flank of the Yuan-An ridge, probably represents thrust faults that extend from seafloor to hydrate-bearing layer. We suggest that the BSR has been disturbed by the thrust faults and further rupture of the fault could potentially trigger failures in the study area.

1. INTRODUCTION

Convergent margins are responsible for the most destructive of earth's plate tectonic processes. Earthquakes and tsunamis in the collision/subduction zone are responsible for human deaths and huge economic losses per year. Earthquakes are a major trigger of submarine landslides that they can cause rapid accelerations, stress the sediment, and tectonic loading to create excess fluid pressuring (Hampton et al. 1996; Hsu et al. 2008). In the offshore region, slope instability is enhanced in subduction zones where faulting and large magnitude earthquakes associated with plate subduction may promote slope failure (e.g., Li and Clark 1991). On the other hand, submarine landslides should be extensive geomorphic evidence of erosion on a convergent margin that induces giant earthquakes (Hampton et al. 1996; McAdoo et al. 2000, 2004). For example, a tsunami generated by a submarine landslide devastated coastal regions of Papua New Guinea after the 17 July 1998, magnitude 7 Sissano earthquake had been reported (Tappin et al. 2001). McAdoo et al. (2004) proposed that the Cascadia seafloor has a very delicate bathymetry, with well-preserved landslides and covered slopes, with a potential to generate M~9 earthquake. Although the instability of submarine slopes may vary significantly with the extent of the slope and the complexity of the bathymetry (Sultan et al. 2001), increased attention has been paid to submarine slope instability for the offshore, southwestern Taiwan. The accretionary prism offshore of southwestern Taiwan is tectonically very active (Huang et al. 1997; Lacombe et al. 2001; Liu et al. 2004), moderate convergent rates (~4 cm yr^{-1}) (Ching et al. 2007), and has received large amounts of sediments from the Taiwan mountain belt (Covey 1984; Milliman and Kao 2005;

* *Corresponding author*
E-mail: wbin@just.edu.tw

Lin et al. 2008). The high deformation intensity in southwestern Taiwan (Chang et al. 2003) is analog to the Cascadia subduction zone.

In order to increase our understanding on the risk of marine slope instability of the accretionary prism offshore southwestern Taiwan, we must use all tools at our disposal. Wide-angle seismic reflection has proven a useful geophysical tool to investigate landslides (e.g., Brooke 1973; Bogoslovsky and Ogilvy 1977). The velocity structure of a landslide mass, the depth to the failure surface, and the lateral extent of a landslide are variables that may be estimated using wide-angle seismic reflection. Lateral and vertical changes in velocity, steeply dipping and discontinuous refractors, and diffractions from blocks within the landslide mass are features commonly observed in wide-angle reflection surveys of landslides (Abramson et al. 2002). In the April of 2014, we carried out an Ocean Bottom Seismometer (OBS) survey in the vicinity of the Yuan-An and Good Weather ridges (Fig. 1), located not only above a potential deep-seated hydrocarbon reservoir (Liu et al. 2006; Chen et al. 2018) but also a crucial study area for understanding potential geohazards (Su et al. 2015, 2018). The aims of this study are to utilize four-component OBS data to determine local two-dimensional (2D) P- and S-wave velocity models of the wide-angle reflection profile and to characterize the lithology in the subsurface.

2. GEOLOGICAL SETTING

Offshore of southwestern Taiwan is an area where the Manila subduction system transforms into an incipient are-continent collision system from south to north (Fig. 1). The prominent morphological features are a series of north-south-trending ridges and troughs (Fig. 1). Two tectonic provinces, the passive China continental margin province and the active accretionary wedge province, are separated by a deformation front (Liu et al. 1997, 2006).

Camerlenghi et al. (2010) reviewed the important observation that large landslides are common along seismically inactive Mediterranean continental margins, and that currently fewer large slope failures occur along tectonically active margins (e.g., McAdoo and Watts 2004) than along passive continental margins (e.g., Ten Brink et al. 2006). The Yung-An Ridge is a structural high located in the active accretionary wedge province of the collision system offshore southwestern Taiwan (Fig. 1). Morphological and structural characters are ridges formed by west-vergent thrusts and folds, and their associated slope basins. Chuang et al. (2013) obtained the highest iodide concentrations in the three ridges (Tainan, Yung-An, and Good Weather). The depth-integrated anaerobic oxidation of methane and sulfate reduction rates were more comparable and were similar to sites studied in the Black Sea, Sea of Okhotsk, and the Namibian shelf where upward fluid flow is absent (Chuang et al. 2013). By integrating marine geophysical results together with geological and geochemical information derived from analyzing core samples, Chiu and Liu (2008) suggest that the Yung-An Ridge area may possess three different types of gas hydrate reservoirs. Wide spread occurrence of bottom simulating reflectors (BSRs) observed in the Yung-An Ridge area indicated the presence of gas hydrates and thus sufficient supply of methane and water (Liu et al. 2006; Hsu et al. 2018b). Based on the BSR arrival times, sub-bottom depth, and associated heat flow, Schnürle et al. (2006) suggested that the local structure plays an important role in the gas hydrate emplacements. The presence of mud volcanoes both offshore (Chiu et al. 2006; Chen et al. 2018) and onshore in Taiwan (Yang et al. 2004) indicates active fluid

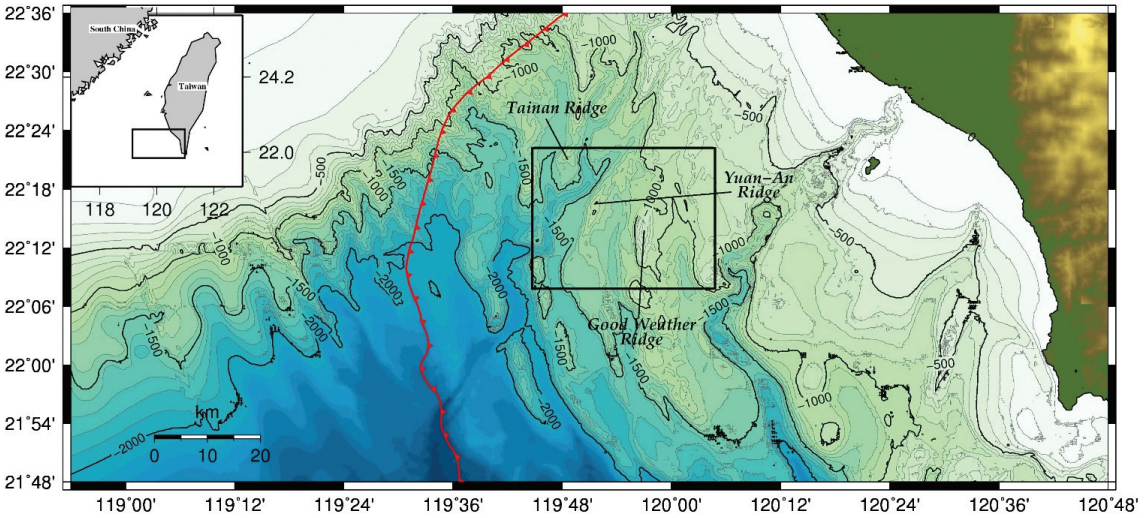

Fig. 1. Shaded relief map with a contour interval of 200 m and the location of study area off southwest Taiwan. The box shows the area of seismic experiment.

expulsion in the accretionary wedge. Chemical analyses of the gases from onshore mud volcanoes (Yang et al. 2004) suggested that most of the gas originates from deeper crust. BSRs are widely recognized in this region, with active fluid migration from seismic data and observed from authigenic carbonate deposits and other geochemical evidence on the seafloor (Yang et al. 2006). Because of these strong hydrate-related signatures, the Yung-An Ridge has been proposed as a high priority drilling site for gas hydrate investigations.

3. SEISMIC DATA

The Yuan-An survey site lies in a water depth of about 1400 m on the active accretionary wedge southwestern Taiwan. In the April of 2014, a joint OBS wide-angle reflection and refraction and multi-channel seismic (MCS) reflection experiment was conducted offshore southwestern Taiwan. Twenty French IFEMER's OBS were deployed in the vicinity of the Yuan-An and Good Weather ridges (Fig. 2). One of the French IFEMER's OBS was not recovered during the cruise. The OBSs recorded data at 4 ms sampling interval from a three-component set of 4.5 Hz geophones and a hydrophone. Time drift rate of the recorded seismic data is less than 1 ms per day using a precise clock.

The airgun source consisted of two GIguns, configures at 545 in^3, which were towed at ~3 m depth and was triggered at a 10 s interval at about 4 knots yielding spaced seismic traces of about 25 m. Airgun firing times on the R/V Research III were determined from the airgun fire command time as measured on a Global Positioning System (GPS) clock. Origin times of the airgun array are believed to be accurate to within a millisecond. Navigation of the R/V Research III was also achieved using a GPS receiver. The airgun shot locations represent locations for the midpoint of the airgun array having been corrected for the offset between the GPS antenna and the airgun array.

We then perform 2D inversion of the reflected and refracted arrivals of the inline shots of this OBS transect. The pre-processing sequence of the OBS records includes OBS relocation and geometry, band-pass filter, spiking-predictive deconvolution (the operator is mixed along 5 adjacent traces), time-offset variant gain, and a low-cut band-pass filter in order to enhance the reflected arrivals. The in-line multi-channel seismic profile MCS1073B, depth migrated with a constant 1480 m s^{-1} acoustic velocity above the sea-floor and a vertical velocity gradient of about 0.8 m s^{-1} below, is used to generate the initial model. To obtain the accurate location of an OBS on the seafloor, we applied an inversion algorithm (West 2001) which uses the travel time of the direct arrival, a water velocity profile, an initial assumed water depth for the OBS and an initial location based on sea-surface deployment and recovery positions. We also assumed that the clock time drift is small and linear over the period of airgun operation. Derivatives of the travel-time misfits with respect to

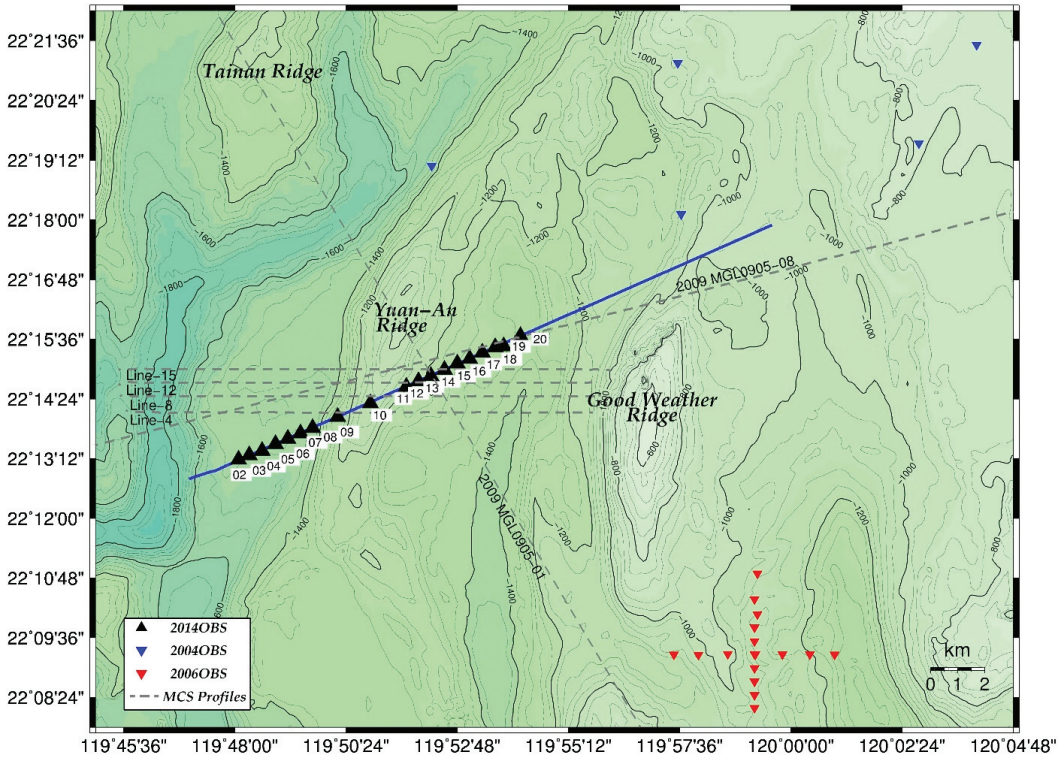

Fig. 2. Shaded relief map and the seismic ship tracks (blue lines) off southwest Taiwan. Open triangles indicate relocated ocean bottom seismometers (OBS). The bathymetric contour interval is 100 m.

changes in location and timing can then be inverted to find the best–fit OBS location and clock corrections.

In addition to the sea-floor, BSR and first-arrivals, we also pick 2 reflectors, PS1 and PS2 within the sediments above the BSR (Figs. 3 and 4). Ray tracing of acoustic as well as converted wave arrivals is performed with the 2-D Rayinvr software, developed by Zelt and Smith (1992). The velocity model is layer based, with coordinal nodes extracted from the digitized horizons and sampled every 100 m, and velocity nodes sampled every 400 m. For each OBS, we then performed ray tracing of the refracted acoustic waves and the reflections arising at the initial model's interfaces. These modeled arrivals are then used to identify their observed time on the OBS records. A damped least-square to the linearized inverse problem (Zelt and Smith 1992), using the partial derivatives of the travel times with respect to the model parameters and the travel time residuals is used to invert the acoustic velocities on the OBS transect. We perform iterations in a layer-stripping approach: bottom velocities at the base of layer 1 to sedimentary layers below BSR are inverted with a smooth damped least square. The RMS travel-time misfits (in milliseconds)/normalized chi-squares for each layer are shown in Table 1.

4. VELOCITY ANALYSIS

To aid the identification and picking of arrivals, the OBS record traces were time shifted to flatten the direct water arrival to arrive at about the same time for all shot offsets. The water velocity and the theorectical travel time were manually adjusted to make the arrival time as constant as possible for all offsets (Fig. 3).

4.1 P-Wave Data Evaluation

The first arrivals, BSR and P1 and P2 arrivals were picked in hydrophone and vertical components of OBS data across the whole survey area (Fig. 3). The travel times of BSR picked from multi-channel seismic profiles were also used. Since BSR picks are densely distributed in the central region of our study area, the velocity model between the sea floor and the BSR is considered resolved well where the depth of BSR is well constrained. Pick uncertainties ranged from 4 - 30 ms for the OBS data depending on signal-to-noise ratio.

4.2 PS-Converted Wave Data Evaluation

P-S converted waves are generally easy to identify because they form almost flat arrivals approximately to the water arrivals (Fig. 4). Westbrook et al. (2008) demonstrated that the only large-amplitude P-S conversions are for P-waves entering the sediments and being converted to S-waves on reflection from interfaces within the sediments and from the BSR based on synthetic modeling. To simplify the process and reduce uncertainty, we chose to use only converted waves from boundaries with large changes in physical property across sediments and BSR (Fig. 4). Because the ray paths of the upgoing mode-converted S-waves are very nearly vertical, the observed P-S converted waves were picked on the vertical and horizontal components of the seismograms in this study.

Once the best-fitting P-wave model was found, S-wave velocities were derived using the optimal Vp model and varying Poisson's ratio for each layer to obtain the best-fit between the calculated and observed travel times using Rayinvr software (Zelt and Smith 1992). The Vp/Vs ratio is determined by correlating P-wave reflections on the hydrophone and vertical components with PS-wave reflection on the horizontal component that originate from the same interface. A single value of Poisson's ratio for each block was then chosen and varied until rays traced through the model matched the observed traveltimes of the P-S converted waves.

5. RESULTS AND DISCUSSION

We used both the four components of OBS data to obtain the seismic velocities of the sediments by travel-time inversion. A total of 1409, 8614, and 8839 arrival-times are digitized for first arrival, P-wave reflection and PS-converted wave, respectively. The RMS travel time residuals for the P-wave reflection pickings ranged from 0.04 - 0.067 s and from 0.08 - 0.086 s for the PS-converted wave arrivals (Table 1). Generally, a good match was obtained between calculated and observed traveltimes. We plot Vp models of study area in vertical slices in Fig. 5. It shows that the velocity contours in the upper part of sediments below the seafloor in good spatial agreement with stratigraphic reflectors revealed in MCS profiles. Sea floor P-wave velocities are about ~1580 m s^{-1}, increasing to the BSR, reaching values of ~2030 m s^{-1} immediately above. Below it, a low velocity layer (1.62 - 1.74 km s^{-1}) is observed, which indicates the presence free gas in the sedimentary layer. However, the picking of the base of the free gas layer was particularly uncertain, so that these arrivals are not considered in the inversion procedure. Therefore, the blue area about 2.2 km in depth on the western part of Fig. 5a should be artifacts in velocity models as they derived from arrivals with moderate picking errors.

The results for the Vs model of study area are presented in vertical slices as shown also in Fig. 6. Values of the S-wave velocities of the sea floor are about 300 m s^{-1}, with a uniform increase with depth through the region of the BSR, reaching values of ~610 m s^{-1} immediately above. The dominant feature in the S-wave velocity model is a lateral velocity variations under the western flank of the Yuan-An ridge above the BSR (Fig. 6). It is commonly believed

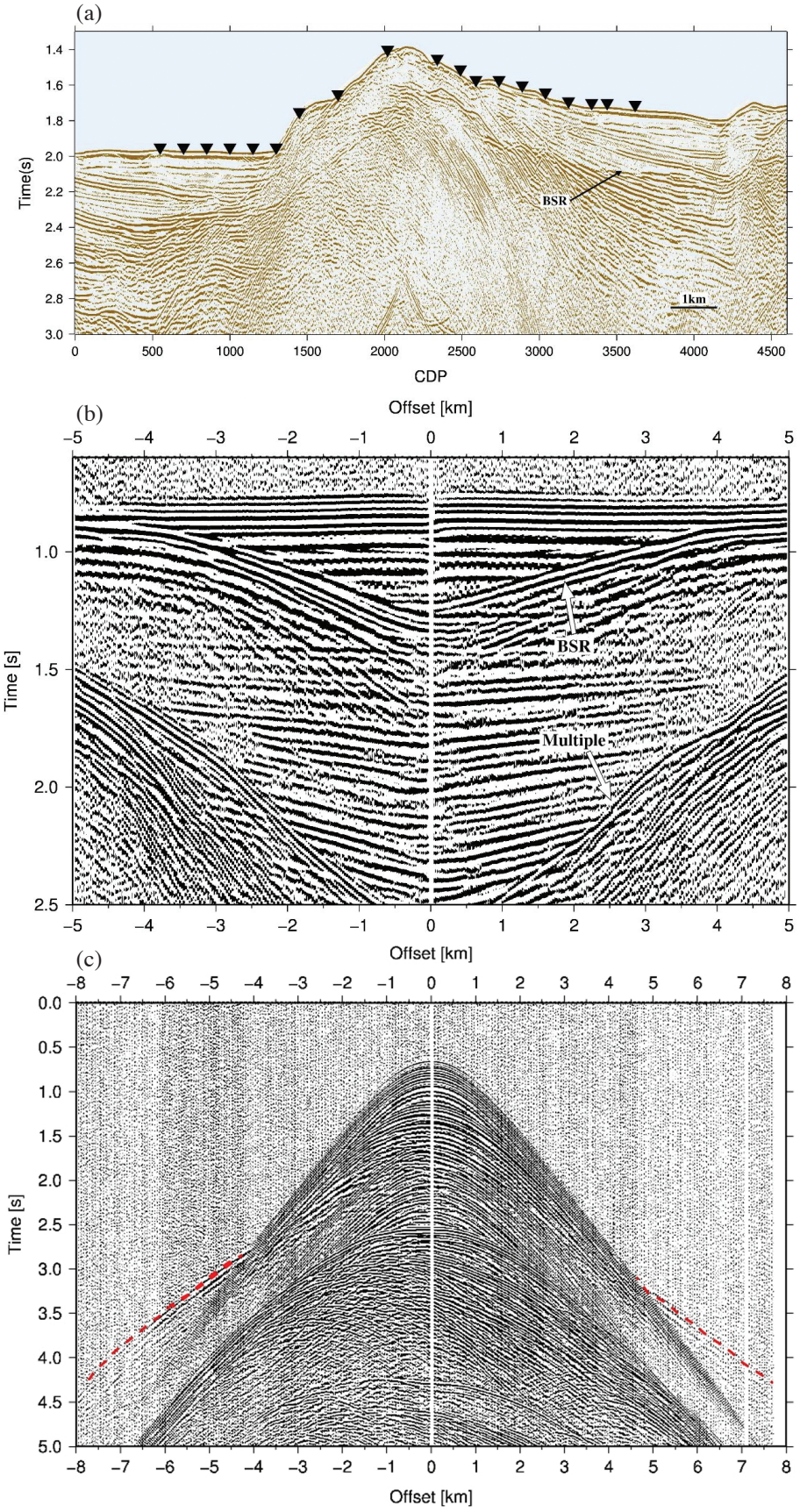

Fig. 3. Representative MCS and OBS record sections. (a) The multichannel reflection profile. Solid inverted triangles indicate relocated ocean bottom seismometers (OBS). (b) Vertical channel of OBS18 displayed with the direct arrival flattened. (c) First arrivals (red dotted lines) picked from the vertical channel of OBS16.

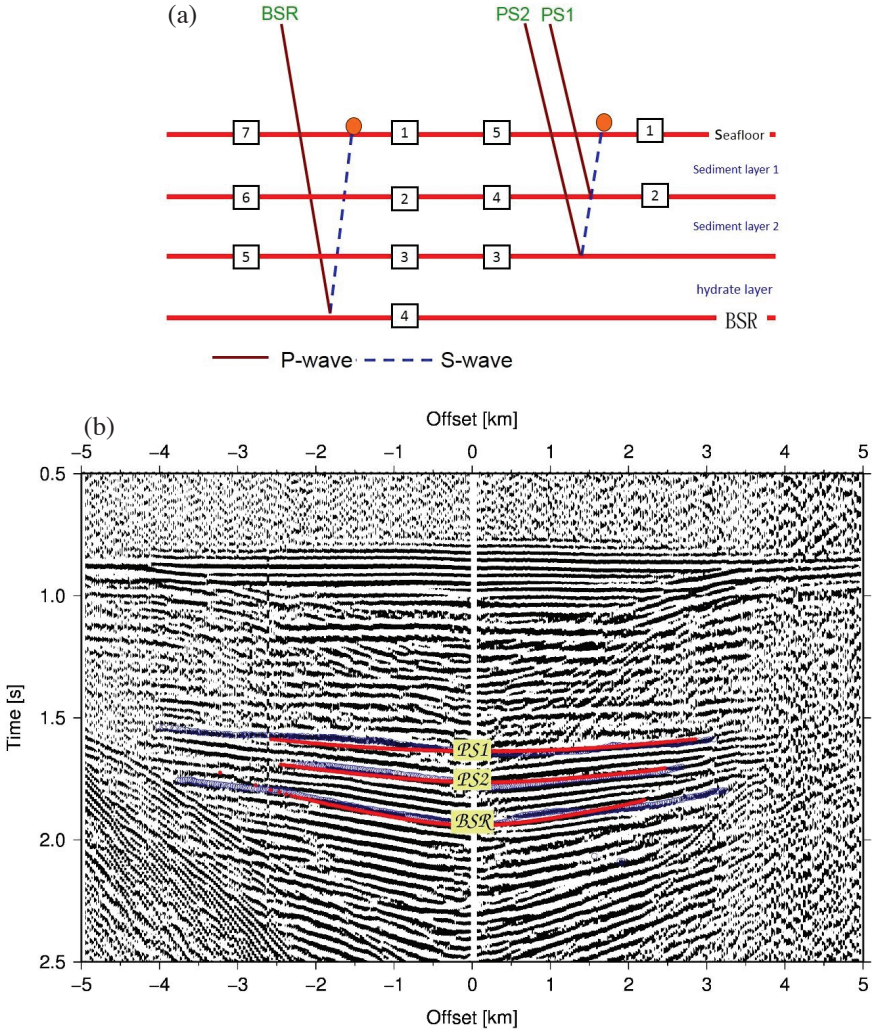

Fig. 4. (a) Ray paths of P-S converted waves travelling from the airgun sources at the sea surface and reflected from sedimentary layers (PS1 and PS2) and the bottom simulating reflectors (BSR). (b) Horizontal channel of OBS20 displayed with the direct arrival flattened. Reflected S-waves generated by P-S conversion at PS1, PS2, and BSR.

Table 1. Misfit Statistics of the Velocity Modeling. (a) P-wave; (b) Converted PS-wave; (c) P-wave refraction.

(a)

Number of OBS	Phase	Number of Arrival Picks	t_{RMS} (s)	x^2
19	Refletion P arrivals (Layer 1)	2440	0.040	0.321
	Refletion P arrivals (Layer 2)	2721	0.043	0.187
	BSR arrivals	3453	0.067	0.916
	Overall	8614	0.050	0.474

(b)

Number of OBS	Phase	Number of Arrival Picks	t_{RMS} (s)	x^2
19	Converted PS arrivals (Layer 1)	3146	0.080	0.645
	Converted PS arrivals (Layer 2)	2685	0.086	1.506
	Converted PS arrivals (BSR)	3008	0.083	1.391
	Overall	8839	0.083	1.180

(c)

Number of OBS	Phase	Number of Arrival Picks	t_{RMS} (s)	x^2
13	Refraction P arrivals (Layer 7)	1409	0.056	0.315

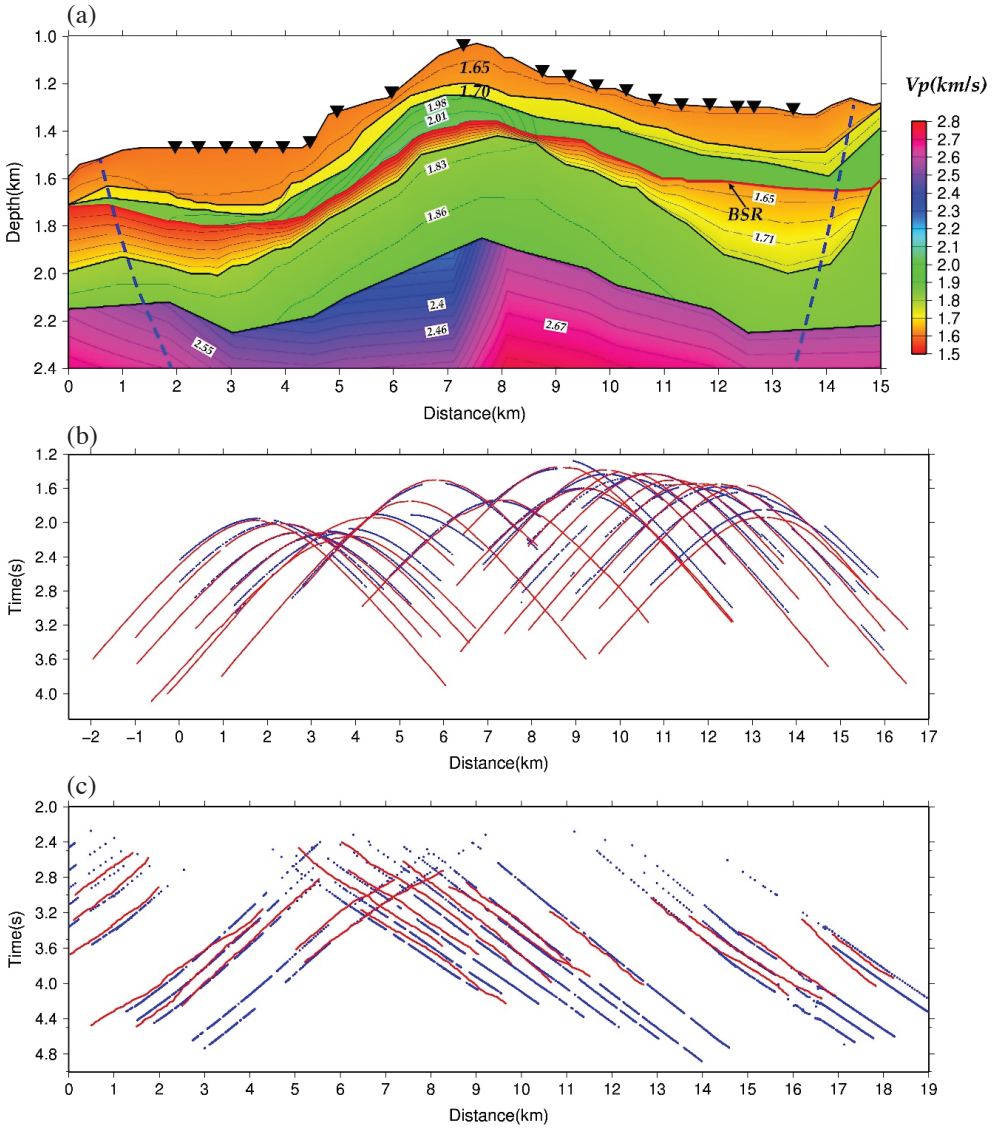

Fig. 5. (a) Cross section of P-wave velocities for profile (location shown in Fig. 2). Solid inverted triangles indicate OBSs. The area inside the blue dotted lines represent well-constrained region. Fit of calculated travel times (red lines) with observed travel times (blue points) for (b) reflection arrivals and (c) refraction arrivals.

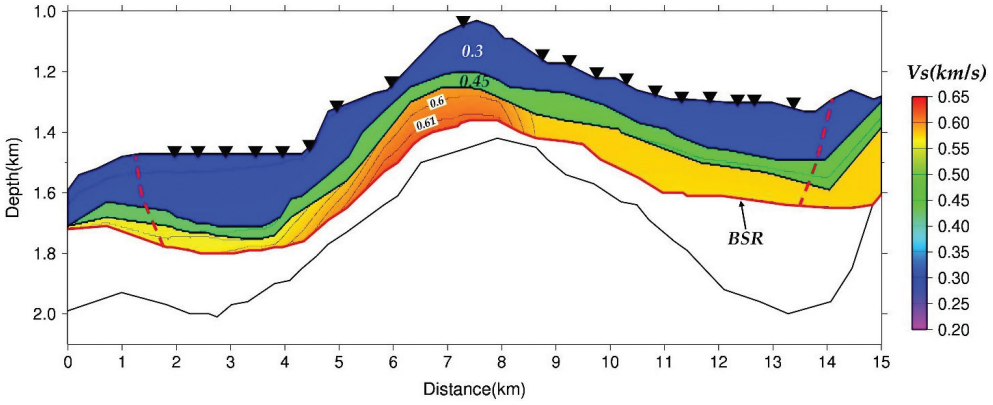

Fig. 6. Cross section of S-wave velocities for profile (location shown in Fig. 2). Solid inverted triangles indicate OBSs. The area inside the red dotted lines represent well-constrained region.

that BSRs are resulted from a decrease in the P-wave velocity from high-velocity layer containing gas hydrate to lower-velocity layer containing a small amount of free gas (e.g., Andreassen et al. 1997; Dovorkin et al. 2000; Tinivella and Accaino 2000). Above the BSR, the solidus phase that fills the clastic matrix creates high P-wave velocities, as well as high S-wave velocities (Figs. 5 and 6).

Several geophysical studies near the Yuan-An ridge had been carried out for the purpose of gas hydrate exploration, particularly multibeam echosounder, OBS seismic reflection/refraction, and side-scan sonar surveys. Schnürle et al. (2006) utilized three independent methods to determine the acoustic and shear-wave velocities of the sediments and investigate the gas hydrate content through rock physic modeling. Cheng et al. (2006) found westward thrusting high velocity wedges along several east-west OBS profiles and suggested them as a series of thrust faults. Schnürle et al. (2011) estimated fluid and gas migration path and intensity for the southern part of the Yuan-An ridge and found that the maximum fluid and gas transport across BSR should occur below the crest of anticlines. Lin et al. (2018) reported a relatively higher fundamental frequency of about 8 - 9 Hz for the more rigid material, such as mud diapir and folding axes. Cheng et al. (2014) estimated gas hydrate saturation by using a modification of Wood's equation and indicated that it varies from 5% at the top ~200 m below the seafloor to 10 - 15% of pore space close to the BSR beneath the Yuan-An ridge. This study is different from previous studies in that the main objective of the present study is to examine possible connections between sedimentary slide features and the presence of gas hydrate beneath the Yuan-An ridge off southwestern Taiwan.

5.1 Thrust Fault and Discontinuous BSR

A series of thrust faults were interpreted on the MCS section (Fig. 7). The faults seems to extend from seafloor to below the current BSR depth beneath the western flank of the Yuan-An ridge. Significant lateral velocity variations are evidenced beneath the area between OBS9 and OBS11 in the hydrate-bearing layer (Fig. 5a). At the western flank, landslide deposit and a large seafloor scarp were observed but the feature of fault cuts through the seafloor is not apparent (Fig. 7). A discontinuous BSR is visible on the MCS seismic section beneath the crest of the Yuan-An ridge. The reflector packages referred to as BSRa are disrupted by these thrust faults (Fig. 7). These anomalous BSR reflections are significantly shallower than the theoretical BSR. The origin of these thrust faults might be associated with stresses in the central uplift region of the Yuan-An ridge, parallel to the ridge orientation and generally perpendicular to the direction of compression produced by ongoing collision. The probable cause for the discontinuous BSR beneath the crest of the Yuan-An ridge is localized fluid flow along these faults. If fluid flow is increased by migration of fluids along those faults, it is possible that the associated increase in heat flow (Chen et al. 2012), and upward migration of the base of methane hydrate stability zone (Chen et al. 2014; Liao et al. 2014), would release methane as to migrate upward and contribute to increasing the concentration of methane hydrate at shallow depth. It is evidence that such an increase of thermal gradient and speculated fluid flow, with faults thrust to the seafloor, have been resulted rough seafloor characters or water column gas flares (Chen et al. 2010). Several of these faults appear to be active since they offset the seafloor near the Yuan-An ridge (Lin et al. 2009), and any further displacement associated with uplift and extension could potentially trigger failures in the study area. However, the interpreted thrust faults and abnormal BSR can be challenged by other scientists. It's suggested to use high resolution bathymetry data or subbottom profiles to help the interpretation of those observations.

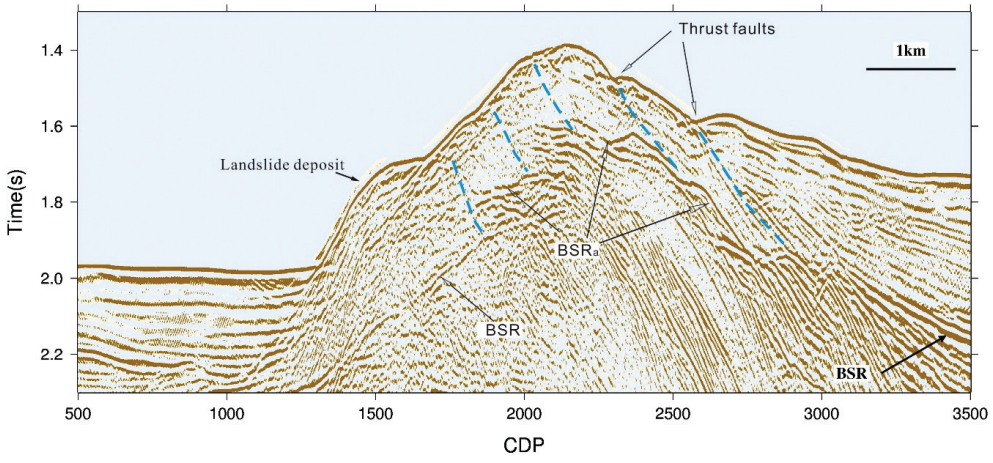

Fig. 7. An enlargement of the Multi-channel seismic section in Fig. 3a. The section shows the depth extent of the thrusts and is generally aligned with clear offsets in the bright reflector near the BSR depth. Label BSRa indicates segments interpreted to be anomalous BSR reflections.

5.2 S-Wave Velocity and Safety Factor

We know that direct S-wave recording is not possible in offshore areas, S-wave velocities were derived from Poisson's ratios. A continuous monitoring of S-wave velocity can warn of impending slope hazard and the overall scope of geotechnical risk assessment (Qureshi et al. 2013). Collett et al. (2009) suggested that many of the encountered drilling hazards were not gas hydrate-related. Issues such as borehole instability, influxes of free gas, drill cuttings removal, and shallow water flow were among the problems faced during an expeditions (Birchwood and Noeth 2012). Drilling-induced compressive rock failure leading to breakouts occurs where the maximum hoop stress is higher than the rock strength (Zoback 2007). Therefore, a big challenge during the drilling campaign was to get optimal data quality by maintaining borehole stability in shallow unconsolidated sediments. The instability of submarine slopes may vary significantly with the extent of the slope and the complexity of the bathymetry. Several studies indicated that the direct values of the internal friction angle and S-wave velocity for marine sediments can be used to develop the relationship between safety factor and S-wave velocity (e.g., Ohta and Goto 1978; Lee 1990; Hasancebi and Ulusay 2006). Based on the Vs model obtained in this study, Hsu et al. (2018a) calculated the safety factors of slope stability along the seismic profile and found that just to the western flank the Yuan-An Ridge attains a minimum value. The prominent landslide deposit found on the western flank of the Yuan-An ridge indicating the slope failure is apparent (Fig. 7).

6. CONCLUDING REMARKS

This paper has demonstrated the valuable results from using four-component ocean bottom seismometers on the seabed for measurement of P- and S-wave properties, which provide additional information to assess the marine slope stability at the seabed. We image the P-wave velocity structure of the sediments and thereby estimate S-wave velocities using PS-converted waves collected in an OBS profile across the Yuan-An ridge conducted in 2014. Following conclusions can be reached based on this study:

(1) We inverted Vp from a two-dimensional velocity model. Sea floor velocities are about ~1580 m s^{-1}, increasing to the BSR, reaching values of ~2 km s^{-1} immediately above. S-wave velocities of the sediments over the entire section range from 0.3 to ~0.6 km s^{-1}.

(2) A series of thrust faults were interpreted and a discontinuous of BSR is visible beneath the crest the Yuan-An ridge on the MCS section. We suggest that the BSR has been disturbed by the thrust faults.

(3) Significant lateral velocity variations were found beneath the eastern flank of the Yuan-An ridge which probably represents thrust faults that extends from seafloor to the hydrate-bearing layer.

(4) A prominent feature of landslide deposits just to the western flank of the Yuan-An ridge was observed.

Acknowledgements We are grateful to the scientists and the technologists participating in the cruise during MCS and OBS date acquisition. We thank the editor and two anonymous reviewers for their constructive comments greatly improved the manuscript. This research was supported by the Ministry of Science and Technology, Taiwan under Grant MOST 105-3113-M-008-001 and 104-2116-M-228-001.

REFERENCES

Abramson, L. W., T. S. Lee, S. Sharma, and G. M. Boyce, 2002: Slope stability and stabilization methods, 2nd Ed., John Wiley and Sons, Inc., New York, 712 pp.

Andreassen, K., P. E. Hart, and M. MacKay, 1997: Amplitude versus offset modeling of the bottom simulating reflection associated with submarine gas hydrate. *Mar. Geol.*, **137**, 25-40, doi: 10.1016/s0025-3227(96)00076-x. [Link]

Birchwood, R. and S. Noeth, 2012: Horizontal stress contrast in the shallow marine sediments of the Gulf of Mexico sites Walker Ridge 313 and Atwater Valley 13 and 14 - Geological observations, effects on wellbore stability, and implications for drilling. *Mar. Petrol. Geol.*, **34**, 186-208, doi: 10.1016/j.marpetgeo.2012.01.008. [Link]

Bogoslovsky, V. A. and A. A. Ogilvy, 1977: Geophysical methods for the investigation of landslides. *Geophysics*, **42**, 562-571, doi: 10.1190/1.1440727. [Link]

Brooke, J. P., 1973: Geophysical investigations of a landslide near San Jose, California. *Geoexploration*, **11**, 61-73, doi: 10.1016/0016-7142(73)90049-5. [Link]

Camerlenghi, A., R. Urgeles, and L. Fantoni, 2010: A Database on Submarine Landslides of the Mediterranean Sea. In: Mosher, D. C., R. C. Shipp, L. Moscardelli, J. D. Chaytor, C. D. P. Baxter, H. J. Lee, and R. Urgeles (Eds.), Submarine Mass Movements and Their Consequences, Springer Science + Business Media B.V., 503-514, doi: 10.1007/978-90-481-3071-9_41. [Link]

Chang, C. P., T. Y. Chang, J. Angelier, H. Kao, J. C. Lee, and S. B. Yu, 2003: Strain and stress field in Taiwan oblique convergent system: constraints from GPS observation and tectonic data. *Earth Planet. Sci. Lett.*, **214**, 115-127, doi: 10.1016/s0012-821x(03)00360-1. [Link]

Chen, L., W. C. Chi, C. S. Liu, C. T. Shyu, Y. Wang, and C. Y. Lu, 2012: Deriving regional vertical fluid migration rates offshore southwestern Taiwan using bottom-simulating reflectors. *Mar. Geophys. Res.*, **33**, 379-388, doi: 10.1007/s11001-012-9162-4. [Link]

Chen, L., W. C. Chi, S. K. Wu, C. S. Liu, C. T. Shyu, Y.

S. Wang, and C. Y. Lu, 2014: Two dimensional fluid flow models at two gas hydrate sites offshore southwestern Taiwan. *J. Asian Earth Sci.*, **92**, 245-253, doi: 10.1016/j.jseaes.2014.01.004. [Link]

Chen, S. C., S. K. Hsu, C. H. Tsai, C. Y. Ku, Y. C. Yeh, and Y. Wang, 2010: Gas seepage, pockmarks and mud volcanoes in the near shore of SW Taiwan. *Mar. Geophys. Res.*, **31**, 133-147, doi: 10.1007/s11001-010-9097-6. [Link]

Chen, S.-C., C.-H. Tsai, S.-K. Hsu, Y.-C. Yeh, C.-S. Liu, S.-H. Chung, and C.-Y. Wei, 2018: Fangliao Slide — a large slope failure in the upper Kaoping Slope off southwest Taiwan. *Terr. Atmos. Ocean. Sci.*, **29**, 17-30, doi: 10.3319/TAO.2017.06.14.01. [Link]

Cheng, W. B., C. S. Lee, C. S. Liu, P. Schnurle, S. S. Lin, and H. R. Tsai, 2006: Velocity structure in marine sediments with gas hydrate reflectors in offshore SW Taiwan, from OBS data tomography. *Terr. Atmos. Ocean. Sci.*, **17**, 739-756, doi: 10.3319/TAO.2006.17.4.739(GH). [Link]

Cheng, W. B., T. Y. Shih, W. Y. Lin, T. K. Wang, C. S. Liu, and Y. Wang, 2014: Imaging seismic velocities for hydrate-bearing sediments using converted waves near Yuan-An Ridge, off southwest Taiwan. *J. Asian Earth Sci.*, **92**, 215-223, doi: 10.1016/j.jseaes.2013.10.013. [Link]

Ching, K. E., R. J. Rau, J. C. Lee, and J. C. Hu, 2007: Contemporary deformation of tectonic escape in SW Taiwan from GPS observations, 1995-2005. *Earth Planet. Sci. Lett.*, **262**, 601-619, doi: 10.1016/j.epsl.2007.08.017. [Link]

Chiu, J. K. and C. S. Liu, 2008: Comparison of sedimentary processes on adjacent passive and active continental margins offshore of SW Taiwan based on echo character studies. *Basin Res.*, **20**, 503-518, doi: 10.1111/j.1365-2117.2008.00388.x. [Link]

Chiu, J. K., W. H. Tseng, and C. S. Liu, 2006: Distribution of gassy sediments and mud volcanoes offshore southwestern Taiwan. *Terr. Atmos. Ocean. Sci.*, **17**, 703-722, doi: 10.3319/TAO.2006.17.4.703(GH). [Link]

Chuang, P. C., A. W. Dale, K. Wallmann, M. Haeckel, T. F. Yang, N. C. Chen, H. C. Chen, H. W. Chen, S. Lin, C. H. Sun, C. F. You, C. S. Horng, Y. Wang, and S. H. Chung, 2013: Relating sulfate and methane dynamics to geology: Accretionary prism offshore SW Taiwan. *Geochem. Geophys. Geosyst.*, **14**, 2523-2545, doi: 10.1002/ggge.20168. [Link]

Collett, T. S., R. Boswell, S. Mrozewski, G. Guerin, A. Cook, M. Frye, W. Shedd, and D. McConnell, 2009: Gulf of Mexico Gas Hydrate Joint Industry Project Leg II: Operational Summary: Proceedings of the Drilling and Scientific Results of the 2009 Gulf of Mexico Gas Hydrate Joint Industry Project Leg II. Available at http://www.netl.doe.gov/technologies/oil-gas/publications/Hydrates/2009Reports/OpSum.pdf.

Covey, M., 1984: Lithofacies analysis and basin reconstruction, Plio-Pleistocene western Taiwan foredeep. *Petrol. Geol. Taiwan*, **20**, 53-83.

Dovorkin, J., M. B. Helgerud, W. F. Waite, S. H. Kirby, and A. Nur, 2000: Introduction to physical properties and elasticity models. In: Max, M. D. (Ed.), Natural Gas Hydrate in Oceanic and Permafrost Environments, Kluwer Academic Publishers, Dordrecht, 245-260, doi: 10.1007/978-94-011-4387-5_20. [Link]

Hampton, M. A., H. J. Lee, and J. Locat, 1996: Submarine landslides. *Rev. Geophys.*, **34**, 33-59, doi: 10.1029/95RG03287. [Link]

Hasancebi, N. and R. Ulusay, 2006: Empirical correlations between shear wave velocity and penetration resistance for ground shaking assessments. *Bull. Eng. Geol. Environ.*, **66**, 203-213, doi: 10.1007/s10064-006-0063-0. [Link]

Hsu, H.-H., J.-J. Dong, S.-K. Hsu, and C.-C. Su, 2018: Back analysis of an earthquake-triggered submarine landslide near the SW of Xiaoliuqiu. *Terr. Atmos. Ocean. Sci.*, **29**, 77-85, doi: 10.3319/TAO.2017.05.08.01. [Link]

Hsu, S.-K., J. Kuo, C.-L. Lo, C.-H. Tsai, W.-B. Doo, C.-Y. Ku, and J.-C. Sibuet, 2008: Turbidity currents, submarine landslides and the 2006 Pingtung earthquake off SW Taiwan. *Terr. Atmos. Ocean. Sci.*, **19**, 767-772, doi: 10.3319/TAO.2008.19.6.767(PT). [Link]

Hsu, S.-K., S.-S. Lin, S.-Y. Wang, C.-H. Tsai, W.-B. Doo, S.-C. Chen, J.-Y. Lin, Y.-C. Yeh, H.-F. Wang, and C.-W. Su, 2018: Seabed gas emissions and submarine landslides off SW Taiwan. *Terr. Atmos. Ocean. Sci.*, **29**, 7-15, doi: 10.3319/TAO.2016.10.04.01. [Link]

Huang, C. Y., W. Y. Wu, C. P. Chang, S. Tsao, P. B. Yuan, C. W. Lin, and K. Y. Xia, 1997: Tectonic evolution of accretionary prism in the arc-continent collision terrane of Taiwan. *Tectonophysics*, **281**, 31-51, doi: 10.1016/s0040-1951(97)00157-1. [Link]

Lacombe, O., F. Mouthereau, J. Angelier, and B. Deffontaines, 2001: Structural, geodetic and seismological evidence for tectonic escape in SW Taiwan. *Tectonophysics*, **333**, 323-345, doi: 10.1016/s0040-1951(00)00281-x. [Link]

Lee, S. H., 1990: Regression models of shear wave velocities in Taipei basin. *J. Chin. Inst. Eng.*, **13**, 519-532, doi: 10.1080/02533839.1990.9677284. [Link]

Li, C. and A. L. Clark, 1991: SeaMARC II study of a giant submarine slump on the northern Chile continental slope. *Mar. Geotechnol.*, **10**, 257-268, doi: 10.1080/10641199109379894. [Link]

Liao, W. Z., A. T. Lin, C. S. Liu, J. N. Oung, and Y. Wang, 2014: Heat flow in the rifted continental margin of the South China Sea near Taiwan and its tectonic implications. *J. Asian Earth Sci.*, **92**, 233-244, doi: 10.1016/j.jseaes.2014.01.003. [Link]

Lin, A. T., C. S. Liu, C. C. Lin, P. Schnurle, G. Y. Chen, W. Z. Liao, L. S. Teng, H. J. Chuang, and M. S. Wu, 2008: Tectonic features associated with the overriding of an accretionary wedge on top of a rifted continental margin: An example from Taiwan. *Mar. Geol.*, **255**, 186-203, doi: 10.1016/j.margeo.2008.10.002. [Link]

Lin, C. C., A. T. Lin, C. S. Liu, G. Y. Chen, W. Z. Liao, and P. Schnurle, 2009: Geological controls on BSR occurrences in the incipient arc-continent collision zone off southwest Taiwan. *Mar. Petrol. Geol.*, **26**, 1118-1131, doi: 10.1016/j.marpetgeo.2008.11.002. [Link]

Lin, J.-Y., Y.-F. Chen, C.-C. Su, S.-J. Chin, W.-B. Cheng, W.-N. Wu, C.-W. Liang, H.-S. Hsieh, S.-K. Hsu, and Y.-C. Lin, 2018: Seismic site response of submarine slope offshore southwestern Taiwan. *Terr. Atmos. Ocean. Sci.*, **29**, 51-63, doi: 10.3319/TAO.2017.05.09.01. [Link]

Liu, C. S., I. L. Huang, and L. S. Teng, 1997: Structural features off southwestern Taiwan. *Mar. Geol.*, **137**, 305-319, doi: 10.1016/S0025-3227(96)00093-X. [Link]

Liu, C. S., B. Deffontaines, C. Y. Lu, and S. Lallemand, 2004: Deformation patterns of an accretionary wedge in the transition zone from subduction to collision offshore southwestern Taiwan. *Mar. Geophys. Res.*, **25**, 123-137, doi: 10.1007/s11001-005-0738-0. [Link]

Liu, C. S., P. Schnurle, Y. Wang, S. H. Chung, S. C. Chen, and T. H. Hsiuan, 2006: Distribution and characters of gas hydrate offshore of southwestern Taiwan. *Terr. Atmos. Ocean. Sci.*, **17**, 615-644, doi: 10.3319/TAO.2006.17.4.615(GH). [Link]

McAdoo, B. G. and P. Watts, 2004: Tsunami hazard from submarine landslides on the Oregon continental slope. *Mar. Geol.*, **203**, 235-245, doi: 10.1016/s0025-3227(03)00307-4. [Link]

McAdoo, B. G., L. F. Pratson, and D. L. Orange, 2000: Submarine landslide geomorphology, US continental slope. *Mar. Geol.*, **169**, 103-136, doi: 10.1016/s0025-3227(00)00050-5. [Link]

McAdoo, B. G., M. K. Capone, and J. Minder, 2004: Seafloor geomorphology of convergent margins: Implications for Cascadia seismic hazard. *Tectonics*, **23**, doi: 10.1029/2003tc001570. [Link]

Milliman, J. D. and S. J. Kao, 2005: Hyperpycnal discharge of fluvial sediment to the ocean: Impact of super-typhoon Herb (1996) on Taiwanese rivers. *J. Geol.*, **113**, 503-516, doi: 10.1086/431906. [Link]

Ohta, Y. and N. Goto, 1978: Empirical shear wave velocity equations in terms of characteristic soil indexes. *Earthq. Eng. Struct. Dyn.*, **6**, 167-187, doi: 10.1002/eqe.4290060205. [Link]

Qureshi, M. U., S. Yamada, and I. Towhata, 2013: A simplified technique for slope stability assessment based on insitu S-wave velocity measurement. In: Ugai, K., H. Yagi, and A. Wakai (Eds.), Earthquake-Induced Landslides, Springer-Verlag, Berlin Heidelberg, 871-881, doi: 10.1007/978-3-642-32238-9_95. [Link]

Schnürle, P., C. S. Liu, and C. S. Lee, 2006: Acoustic and shear-wave velocities in hydrate-bearing sediments offshore southwestern Taiwan: Tomography, converted waves analysis and reverse-time migration of OBS records. *Terr. Atmos. Ocean. Sci.*, **17**, 757-779, doi: 10.3319/TAO.2006.17.4.757(GH). [Link]

Schnürle, P., C. S. Liu, A. T. Lin, and S. Lin, 2011: Structural controls on the formation of BSR over a diapiric anticline from a dense MCS survey offshore southwestern Taiwan. *Mar. Petrol. Geol.*, **28**, 1932-1942, doi: 10.1016/j.marpetgeo.2010.12.004. [Link]

Su, C. C., P. H. Tsai, J. T. Liu, S. K. Hsu, and S. D. Chiu, 2015: Impact of Submarine Geohazards on Organic Carbon Burial Offshore Southwestern Taiwan. American Geophysical Union, Fall Meeting, abstract NH23B-1885.

Su, C.-C., S.-T. Hsu, H.-H. Hsu, J.-Y. Lin, and J.-J. Dong, 2018: Sedimentological characteristics and seafloor failure offshore SW Taiwan. *Terr. Atmos. Ocean. Sci.*, **29**, 65-76, doi: 10.3319/TAO.2017.06.21.01. [Link]

Sultan, N., P. Cochonat, J. F. Bourillet, and F. Cayocca, 2001: Evaluation of the Risk of Marine Slope Instability: A Pseudo-3D Approach for Application to Large Areas. *Marine Georesources and Geotechnology*, **19**, 107-133, doi: 10.1080/10641190109353807. [Link]

Tappin, D. R., P. Watts, G. M. McMurtry, Y. Lafoy, and T. Matsumoto, 2001: The Sissano Papua New Guinea tsunami of July 1998 - offshore evidence on the source mechanism. *Mar. Geol.*, **175**, 1-23, doi: 10.1016/s0025-3227(01)00131-1. [Link]

Ten Brink, U. S., E. L. Geist, and B. D. Andrews, 2006: Size distribution of submarine landslides and its implication to tsunami hazard in Puerto Rico. *Geophys. Res. Lett.*, **33**, L11307, doi: 10.1029/2006GL026125. [Link]

Tinivella, U. and F. Accaino, 2000: Compressional velocity structure and Poisson's ratio in marine sediments with gas hydrate and free gas by inversion of reflected and refracted seismic data (South Shetland Islands, Antarctica). *Mar. Geol.*, **164**, 13-27, doi: 10.1016/s0025-3227(99)00123-1. [Link]

West, M., 2001: The Deep Structure of Axial Volcano. Ph.D. Thesis, Univ. of Columbia, New York.

Westbrook, G. K., S. Chand, G. Rossi, C. Long, S. Bunz, A. Camerlenghi, J. M. Carcione, S. Dean, J. P. Foucher, E. Flueh, D. Gei, R. R. Haacke, G. Madrussani, J. Mienert, T. A. Minshull, H. Nouzé, S. Peacock, T. J. Reston, M. Vanneste, and M. Zillmer, 2008: Estimation of gas hydrate concentration from multi-component seismic data at sites on the continental margins of NW Svalbard and the Storegga region of Norway. *Mar. Petrol. Geol.*, **25**, 744-758, doi: 10.1016/j.marpetgeo.2008.02.003. [Link]

Yang, T. F., G. H. Yeh, C. C. Fu, C. C. Wang, T. F. Lan, H. F. Lee, C. H. Chen, V. Walia, and Q. C. Sung, 2004: Composition and exhalation flux of gases from mud volcanoes in Taiwan. *Environ. Geol.*, **46**, 1003-1011, doi: 10.1007/s00254-004-1086-0. [Link]

Yang, T. F., P. C. Chuang, S. Lin, J. C. Chen, Y. Wang, and S. H. Chung, 2006: Methane venting in gas hydrate potential area offshore of SW Taiwan: Evidence of gas analysis of water column samples. *Terr. Atmos. Ocean. Sci.*, **17**, 933-950, doi: 10.3319/TAO.2006.17.4.933(GH). [Link]

Zelt, C. A. and R. B. Smith, 1992: Seismic traveltime inversion for 2-D crustal velocity structure. *Geophys. J. Int.*, **108**, 16-34, doi: 10.1111/j.1365-246x.1992.tb00836.x. [Link]

Zoback, M. D., 2007: Reservoir Geomechanics, Cambridge University Press, 449 pp, doi: 10.1017/cbo9780511586477. [Link]